

Atom Probe Tomography of Organic Molecular Materials: Sub-Dalton Nanometer-Scale Quantification

Andrew P. Proudian,¹ Matthew B. Jaskot,² David R. Diercks,^{2,3} Brian P. Gorman,^{2,4} and Jeramy D. Zimmerman^{1,2}

¹*Department of Physics, Colorado School of Mines*

²*Materials Science Program, Colorado School of Mines*

³*Department of Metallurgical and Materials Engineering, Colorado School of Mines*

⁴*Department of Metallurgy and Materials Engineering, Colorado School of Mines*

(Dated: December 14, 2024)

In this paper, we demonstrate how to apply atom probe tomography (APT) to molecular organic electronic materials. We demonstrate that APT can provide an unprecedented combination of mass resolution of < 1 Da, spatial resolution of ~ 0.3 nm in z and ~ 1 nm in x - y , and an analytic sensitivity of ~ 50 ppm. We detail two systems that demonstrate the power of APT to uncover structure-property relationships in organic systems that have proven extremely difficult to probe using existing techniques: (1) a model organic photovoltaic system in which we show a chemical reaction occurs at the heterointerface; and (2) a model organic light-emitting diode system in which we show molecular segregation occurs. These examples illustrate the power of APT to enable new insights into organic molecular materials.

Keywords: organic photovoltaics; organic light emitting diode; small molecule; morphology; organic electronics; atom probe tomography; local electrode atom probe

CONTENTS

I. Introduction	1
II. Results and Discussion	3
A. Validation	3
B. Organic Photovoltaics	4
C. Organic Light-Emitting Diodes	5
III. Future Directions	6
IV. Conclusions	7
V. Methods	7
A. Sample Preparation	7
B. Data Acquisition and Analysis	7
VI. Acknowledgments	8
VII. Supplemental Information	8
References	8

I. INTRODUCTION

Modern electronics now include a wide variety of organic devices, such as organic photovoltaics (OPVs), organic thin film transistors (OTFTs), and organic light-emitting diodes (OLEDs). Compared to their inorganic counterparts, organic electronic devices enjoy a number of advantages, including low-cost room-temperature deposition, easy patterning at relevant length scales (*e.g.* display pixels), mechanical flexibility, and application-specific tunability; the broad commercial success of OLEDs in the past few years provides a clear example

of this.¹ However, to fully realize these advantages requires more detailed knowledge of the structure-property relationships of these devices. As we will show, atom probe tomography (APT) is a valuable tool for driving our knowledge of these molecular systems.

The fundamental physics of inorganic semiconductors has been well-established for over half a century, though engineering challenges remain. In contrast, there are still many developments to be made in the fundamental physics of organic semiconducting materials.²⁻⁴ A major difference for organic electronics—which makes them more difficult to describe theoretically—is the strong influence of small changes to morphology on device performance and reliability.^{2,5,6} Many methods have been explored to determine how microstructure changes with material, deposition, and processing conditions;^{4,6-15} in addition, morphological changes and molecular degradation impact the performance and lifetime of these devices.^{9,16-22} These studies have led to improvements in performance, but have largely been driven by empirical investigation rather than material theory.⁶⁻⁸ Improved structural characterizations of these devices in three dimensions will lead to better physical theories of organic electronics, shortening development times.^{5-8,23-25}

Because their properties are strongly dependent on morphology, organic films require detailed nanoscale characterization.^{6,24} For inorganic systems, a wide variety of tools are available for high-resolution imaging and tomography.²⁶ Unfortunately, organic systems do not have this luxury, as they are sensitive to ion, electron, and X-ray irradiation, and many techniques are hampered by weak scattering contrast.^{23,24,27-30} This does not rule out these techniques, but limits the kind and quality of data they can yield.

The first major class of techniques that have been employed to ascertain morphology are trans-

mission electron microscopy (TEM) and its derivatives, including high-angle annular dark field scanning TEM (HAADF-STEM), and energy-filtered TEM (EF-TEM).^{5,7,24,25,29,31,32} TEM has enabled ground-breaking studies of organic nanostructures because of its excellent spatial resolution—with some instruments capable of resolving sub-nanometer features—which greatly contributed to the development of organic electronic devices.^{6,23,24} Unfortunately, difficulty with contrast in these systems can make it challenging to definitively identify molecular species.^{23,24,28} Bright-field TEM requires defocusing to create material contrast, which can change the apparent size of features, cause contrast reversals, and lead to quantitative analysis errors.²⁵ EF-TEM or electron energy-loss spectroscopy (EELS) can help with this issue by using energy loss spectra to discriminate materials using a specific element or other spectroscopic signatures.^{23–25,28} However, the spectral response depends on the structure of the sample in addition to its composition, complicating species assignment.²⁸ HAADF-STEM can also improve contrast by looking at high-angle scattered electrons, which depend on the average atomic number, but the reduced electron count leads to a trade-off between signal-to-noise ratio and imaging time (and consequent sample damage).^{24,25} For fullerene systems, endohedral fullerenes have been substituted to increase contrast further, allowing measurement of, *e.g.*, phase purity; however, these systems do not directly reproduce the original system because of changes to the solubility of the endohedral fullerene as compared to the original system.²⁵ Even in native systems with high contrast—such as cyclometallated compounds—it is challenging to determine the three-dimensional structure based on a two-dimensional projection.^{6,31} Electron tomography can overcome this limitation, giving full three-dimensional information; unfortunately, the increased beam exposure due to imaging at many angles exacerbates the material degradation problem of electron microscopy techniques.^{6,23,24} Because of the changes in contrast between the different TEM methods and different sample preparations (*e.g.* sample thickness), comparing and interpreting different results can be challenging.^{6,24}

Scattering methods are also a common tool for probing organic film structure, and have been instrumental in developing our understanding of organic morphologies; but, due to the low scattering contrast or requirement for a tunable source, they must often be performed at beamlines or user facilities.^{7,11,29,32} X-ray reflectometry (XRR) measures layer thickness and roughness, including at buried interfaces, making it a great tool for examining interfacial changes and abruptness; however, it provides no chemical identification.^{7,11} Grazing incidence measurements, such as grazing incidence X-ray diffraction (GIXD) and grazing incidence wide-angle X-ray scattering (GIWAXS), probe three-dimensional morphology, but the former only images crystalline regions and the latter cannot probe the full three-dimensional space of the sample.^{11,24,29,32} Neutron reflectometry (NR) can

measure thicknesses down to a nanometer and is more sensitive to material composition than X-rays, but generally requires deuteration of one organic species.^{9,23,33} Resonant soft X-ray scattering (RSOXS) can examine lateral structures with a thickness of a few nanometers even at buried interfaces, and has higher scattering intensity than hard X-rays through careful selection of the photon energy.^{6,23,32} Scattering methods generally require model fits to interpret the data that are not necessarily unique, but this can be mitigated by using reference materials to provide phase data (*e.g.* phase-sensitive NR).^{6,23}

A variety of other methods have been used to probe nanostructure as well, but these often only provide information within a limited parameter space. One of the most common is atomic force microscopy (AFM), which can characterize surface roughness down to a few nanometers.^{5,7,9,11,23,24,32,34,35} Near-field scanning photocurrent microscopy (NSPM) allows correlation of the surface morphology with photoresponse.^{23,24,36} Complementary to this are various optical techniques—such as UV-vis/IR spectroscopy or spectroscopic ellipsometry—which can image into the bulk of the material but spatially average the information.^{6,7} X-ray photoelectron spectroscopy (XPS) and ultraviolet photoelectron spectroscopy (UPS) can quantitatively identify chemical elements and shifts within ~ 5 nm of the surface, but they have a lateral resolution limit of ~ 30 μm and cannot identify molecular species.⁷ Similarly, near edge X-ray absorption fine structure (NEXAFS) spectroscopy is surface sensitive within ~ 2 nm and has a lateral resolution of 10 nm to 100 nm with the same elemental sensitivity; interpreting this information, however, strongly depends on the interaction model used.^{6,23,24} Time-of-flight secondary ion mass spectrometry (TOF-SIMS) and dynamic SIMS (DSIMS) provide a three-dimensional spatially-resolved chemical profile; however, their lateral resolution is ~ 50 nm—much larger than many morphological features—and the depth resolution from sputtering often must be correlated with a second measurement such as *in-situ* AFM.^{6,7,15,23,35} Furthermore, because the material is sputtered, it generally creates fragments that make interpreting the resultant mass spectrum more difficult, and can have differences in sputtering efficiency for different materials.^{23,37} Even with these limitations, SIMS is closest to a single measurement of chemical and morphological information that is widely used by the community, but still cannot answer many questions about system morphology because of its limited spatial resolution and fragmentation of molecular species.

The immense effort to develop and adopt the aforementioned and other tools has enabled innumerable advances in the field, but many questions remain that are difficult to explore with existing techniques. Existing imaging techniques generally have insufficient resolution or chemical contrast to characterize the nanostructure of the material at adequate levels to inform better physical theories of organic electronics; measurements typically provide either high spatial or sensitive chemical information—but

rarely both—requiring indirect correlation of information from several different techniques.^{23,24}

APT, which combines both high spatial resolution (< 1 nm) and high analytical sensitivity (< 100 ppm) in a comparatively large volume ($> 10^7$ nm³), simultaneously measures chemical and spatial information with high precision.^{38,39} This ability can help provide the structural information needed to propel the next generation of physical theories for organic electronics.

In APT, a sample prepared with a sub-micrometer radius of curvature is held at cryogenic temperatures under high bias, generating a large local electric field. A voltage or laser pulse of adequate intensity excites an atom or molecule on the surface to field evaporate. The electric field accelerates this ion towards a two-dimensional position- and time-sensitive detector; we note that, while the efficiency of this detector is not unity, it can be up to 80% in new instruments,⁴⁰ which is quite high for any ion counting technique.⁴¹ This process repeats until the desired thickness of sample has evaporated. The time-of-flight of each ion gives its mass-to-charge ratio, and its position on the detector allows the ion's location to be reconstructed in three dimensions.^{38,39,42}

Despite APT's excellent spatial and chemical resolution and the relative maturity of the technique, the body of APT analyses of organic systems is small.^{43–51} Most of these studies looked at polymers, which, because of their chain structure, fragment during field evaporation.^{47–51} In 2012, Joester *et al.* examined a blend of poly(3-hexylthiophene-2,5-diyl) (P3HT) and C₆₀,⁵¹ as before, the P3HT polymer proved difficult to study due to uneven fragmentation, but the mass-spectrum had a clear C₆₀ signal, suggesting that small-molecule organic systems should be amenable to study with APT.

In this paper, we show that APT has a mass resolution of < 1 Da, spatial resolution of ~ 0.3 nm in z and ~ 1 nm in x - y , and an analytic sensitivity of ~ 50 ppm. This capability enables new insights into structure-property relationships at the nanoscale—both at interfaces and in the bulk—which we demonstrate in an OPV and an OLED system. This information can help drive forward the development and deployment of molecular organic electronics.

II. RESULTS AND DISCUSSION

Organic molecular materials span a wide range of structures, bond types, masses, and atomic constituents. This variety makes organic electronics very versatile, but also challenging to assign properties as a whole group. We have successfully analyzed a number of materials systems with APT that represent a reasonable cross-section of common organic electronic molecular classes; some of these structures are shown in Figure 1, and other materials include bathophenanthroline (BPhen), diindenoperylene (DIP), and 4-(dicyanomethylene)-2-methyl-6-julolidyl-9-enyl-4H-pyran (DCM2). Thus far

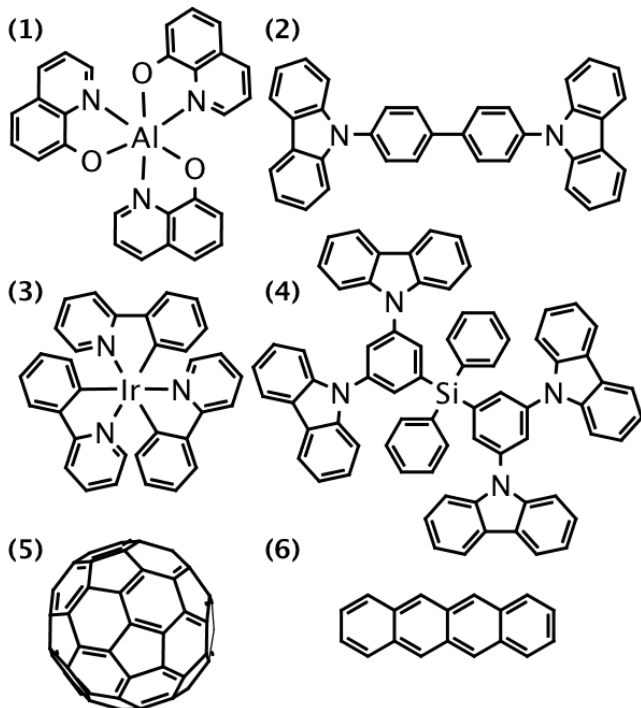


Figure 1. Some example molecules successfully analyzed with atom probe: (1) tris-(8-hydroxyquinoline)aluminum (Alq₃), (2) 4,4'-bis(N-carbazolyl)-1,1'-biphenyl (CBP), (3) tris[2-phenylpyridinato-C₂,N]iridium(III) (Ir(ppy)₃), (4) bis[3,5-di(9H-carbazol-9-yl)phenyl]diphenylsilane (SimCP2), (5) C₆₀, (6) tetracene.

we have confined ourselves to thermally evaporable molecules, but this is not a known limitation of the technique; in fact, in electron irradiated systems we observe field evaporation of covalently bridged C₆₀ dimers and trimers, which are both insoluble and cannot be sublimed. The limits for applicability of APT to organic and other materials systems are not fully known, and merit further study. The Methods section provides details of our sample preparation and analysis process.

In applying a new technique to any system, it is important to understand the quality of information it provides. For APT, there are three major concerns: (1) species discrimination, (2) molecular fragmentation, and (3) spatial resolution. We address each of these to validate APT for organic molecular materials.

A. Validation

In APT, mass resolution is typically characterized by the mass resolving power (MRP), which is given by:⁵²

$$MRP = \frac{m}{\Delta m} \quad (1)$$

where Δm is the full-width at half-maximum of the peak at mass m . We have demonstrated MRPs of > 1000 using a flight path length of 160 mm; Figure 2 shows part of

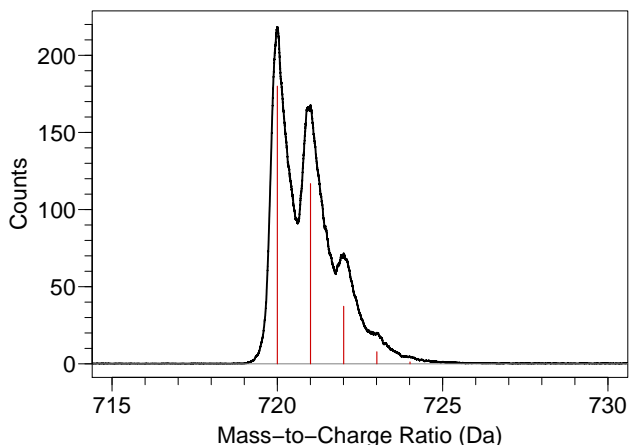


Figure 2. Mass spectrum of C_{60}^+ showing isotopic peaks; the red lines are its expected isotopic distribution. Based on the peak separation, this spectrum has a mass resolving power ($m/\Delta m$) of about 1000.

a mass spectrum collected on a sample of C_{60} (structure shown in Figure 1 (5)) in which the isotopic peaks are clearly resolved. This high MRP allows definitive identification of the molecular constituents of a sample by comparing the spectrum to the expected isotope distribution.

Figure 3a shows the mass spectrum of a blended film of 6 vol % tris[2-phenylpyridinato-C₂,N]iridium(III) ($Ir(ppy)_3$) in 4,4'-bis(N-carbazolyl)-1,1'-biphenyl (CBP, purified by thermal gradient sublimation) (their molecular structures are shown in Figure 1 (2) & (3)). There is a small but clearly resolvable peak at 319 Da (marked Impurity); that we can observe this peak at all is a clear advantage of APT in organic systems, as it comprises only $\sim 0.5\%$ of the total film. This peak is near the mass of CBP missing one carbazole group, and therefore might be thought to arise from the fragmentation of the molecule during the atom probe evaporation process; however, the high MRP of APT allows us to discern that this peak is 1 Da too heavy for a fragment with a dangling bond, indicating that there is a hydrogen attached to the phenyl ring. This extra hydrogen identifies this peak as an impurity in the material left over from its synthesis, not a fragment. We note that the nearby $Ir(ppy)_3^{++}$ peak is at the expected mass and can be used as a reference.

APT provides more data than just spatial position and mass, and this ancillary information can reveal more about what has been observed. Because of both the dynamic distribution of the electric field on the sample's surface and the stochastic nature of field evaporation events, multiple ions can evaporate during the same pulse.⁵³ This is sometimes reduced through the selection of run parameters, but these multiple hit events can enhance our interpretation of the data. A 2D correlation histogram of double hit events during an APT run (Figure S1) shows no evidence of molecular fragmentation

during ionization of the $Ir(ppy)_3:CBP$ sample, strengthening our rejection of fragmentation.⁵⁴ Furthermore, a run of as-received CBP shows this impurity comprising about 5 % of the film (Figure S2 in the Supporting Information), further supporting the impurity interpretation of these peaks.⁵⁴ Given the noise floor observed in these spectra, we estimate our sensitivity to be approximately 50 ppm.

Because the sample acts as the optic and we use an unconventional tip geometry in this implementation (see Methods section), it is critical to characterize the spatial resolution. To test our spatial resolution, we prepared a film of C_{60} on DIP, which templates C_{60} with the (111) plane parallel to the substrate and enhances crystallinity.⁵⁵ The crystalline structure provides an internal measure of the spatial resolution of APT for our specimens, which has been the standard method of estimating resolution among the APT community.⁵⁶

Figure 4 shows the film's z-axis spatial distribution map (SDM)—a common analysis method for crystalline APT data that measures the distribution of z-axis components of the vectors between points in a neighborhood.⁴¹ Fitting to a model of evenly spaced Gaussian functions with equal standard deviations allows us to extract information about our resolution. The regular spacing of the peaks is 0.817(2) nm with this reconstruction, which corresponds to the expected (111) lattice planes of the oriented C_{60} at 0.817 nm. The width of the peaks indicates that the spatial resolution of this sample—which we define as the standard deviation of the fitted Gaussians—is 0.313(3) nm in the z-direction. We note that this is not a physical limit of the resolution for the technique, but what was achieved for this particular sample; we discuss ways to improve this resolution in the Future Directions section.

Given this known dimension in z, we can adjust the reconstruction parameters to return the expected density of the crystal. This reconstruction allows for estimation of the field of view, which for this sample is around 760 nm; as there are about 800 pixels across the detector,⁵⁷ our x-y resolution is limited to about 1 nm but could be improved with different sample geometries or increasing the detector path length from 90 mm to 160 mm. A real space plot of molecular locations is provided in the Supporting Information (Figure S4).

B. Organic Photovoltaics

In 2016, we used APT to investigate the behavior of the bilayer fullerene/acene small-molecule OPV system—one of the most studied models for testing our understanding of the crucial heterojunction interface for OPVs.⁵⁸ APT revealed that the fullerene and acene molecules chemically react at the heterojunction interface, creating a partial monolayer of a Diels-Alder cycloadduct (DAC) species (Figure 5a) that standard processing techniques cannot eliminate. This spatially resolved chemical reso-

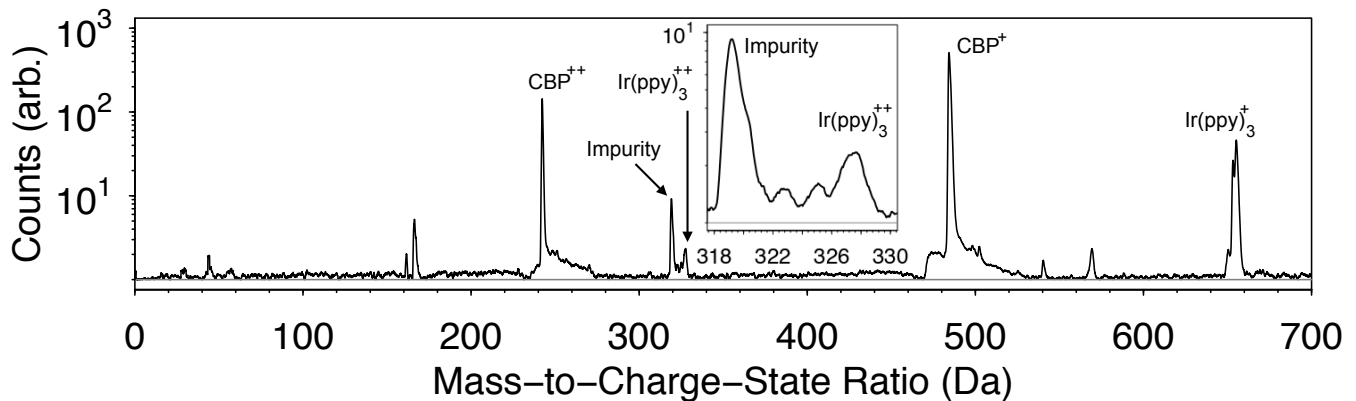


Figure 3. Mass spectrum of a blended film of 6 vol % Ir(ppy)₃ in CBP; (inset) Region of CBP impurity showing a clear offset of 1 Da from the expected fragment location, while the Ir(ppy)₃⁺⁺ peak is at its expected mass.

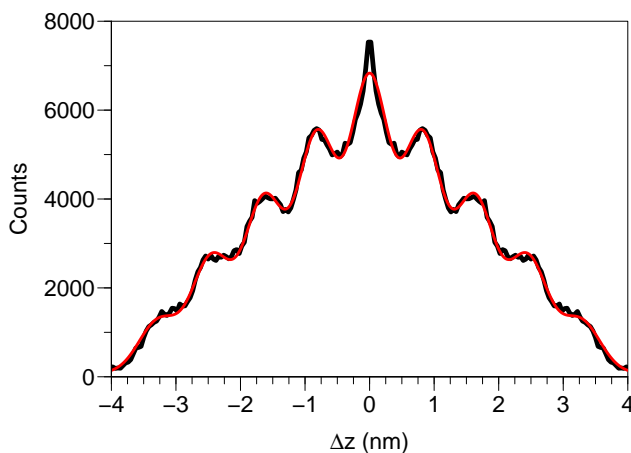


Figure 4. Spatial distribution map (SDM) of C₆₀ templated on diindenoperylene (DIP) showing crystal planes in the z direction. The sampled volume is $\sim 2600 \text{ nm}^3$. A fit to the peaks (red) indicates the spatial resolution of this sample in the z dimension is 0.313(2) nm.

lution helps explain changes in device performance due to the presence of the DAC.

Though this adduct might be attributed to a van der Waals bonded pair of C₆₀ and tetracene (Tc; structure in Figure 1 (6)) co-evaporating, measuring a blended film of C₆₀:Tc with Fourier transform infrared (FTIR) spectroscopy confirms the presence of vibrational modes previously attributed to the Diels-Alder cycloadduct, which provides strong evidence for a reaction.⁵⁹ We also note that Breuer *et al.* concurrently observed the presence of a reaction at the interface.⁶⁰

Because the DAC has a lowest unoccupied molecular orbital (LUMO) energy $\sim 0.16 \text{ eV}$ shallower than C₆₀, the presence of the DAC at the interface should affect device properties by preventing electrons from reaching the interface.⁶¹ To test the effects of the DAC on device parameters, we purposefully introduced an “interlayer” of DAC by co-depositing a Tc:C₆₀ blend at the interface

and performed an annealing series to vary the extent of the interfacial reaction. The data in Figure 5b demonstrate that the reaction does indeed change device properties: the devices with the co-deposited interlayer show higher open circuit voltage (V_{OC}) than the bilayer devices. Furthermore, the increase of V_{OC} with annealing temperature in all devices corresponds to an increase in the DAC as measured by FTIR. This information, combined with temperature-dependent external quantum efficiency and V_{OC} measurements, allowed us to determine that—because face-on Tc/C₆₀ interfaces have the smallest CT-exciton energy⁶² and are the most reactive⁶³—these sites should form the DAC first upon annealing, removing the deepest traps sites from the density of states at the heterointerface. This reduces the average reorganization energy for CT exciton formation, consequently increasing V_{OC} .

This problem takes advantage of APT’s strengths: there is no elemental composition change for this species, and its concentration and location in the film are critically important to understanding its impact on device performance. The development of this analysis, and the explanation that resulted, was only possible because of the unique capabilities of APT. Measuring the clear structure-property relations of an organic system moves the field closer to closing the experiment-theory loop.

C. Organic Light-Emitting Diodes

In fluorescent and phosphorescent systems such as OLEDs, high enough local concentrations of the emitter molecule cause concentration quenching—an issue where a sufficient dimer concentration allows for rapid non-radiative relaxation to the ground state, reducing efficiency.^{64,65} The first report of concentration quenching in OLEDs was by Tang, Vanslyke, and Chen⁶⁶ two years after their seminal paper describing efficient organic electroluminescence.⁶⁷ This concentration effect impacts both efficiency and peak emission wavelength,

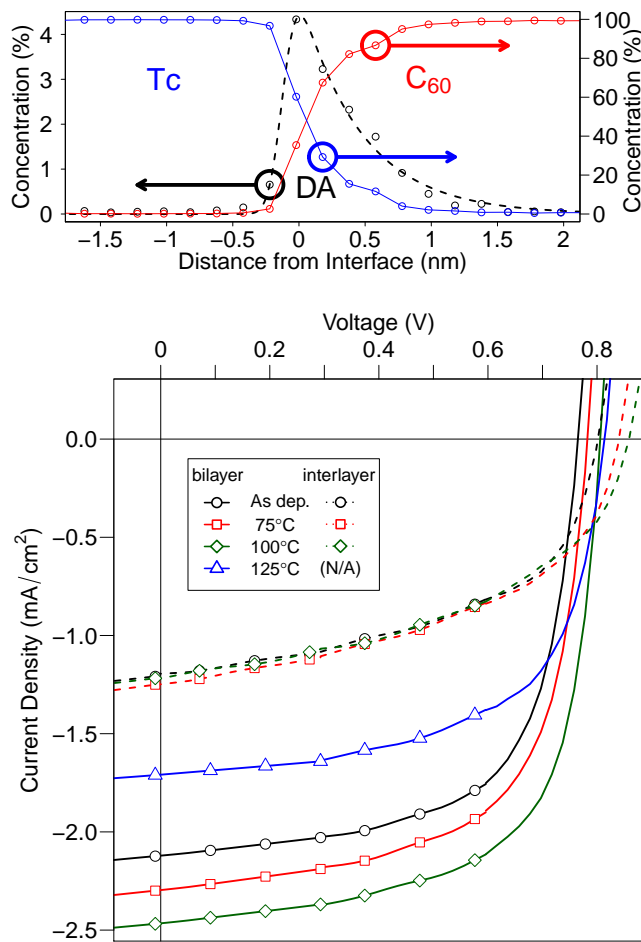


Figure 5. (a) Molecular concentration profile near the interface of the C_{60} -tetracene (Tc) planar heterojunction. The concentration of the Diels-Alder adduct is confined to the interface. (b) Representative current density-voltage (J - V) curves for Tc/ C_{60} bilayer devices under 1 sun illumination (AM1.5), tested as-deposited and after annealing at 75 °C, 100 °C and 125 °C for 30 min (solid lines). Equivalent devices with a 10 nm Tc: C_{60} interlayer are also shown in dashed lines with symbols and colors that correspond to annealing conditions for the bilayer devices. Adapted with permission from *Nano Lett.*, 2016, **16** (10), pp 6086–6091.⁵⁸ © 2016 American Chemical Society.

and is compounded for systems in which the guest emitter molecule aggregates.³¹

The heavily-studied, archetypal phosphorescent OLED system of CBP:Ir(ppy)₃ is suspected of this emitter aggregation, increasing self-quenching, exciton-exciton and exciton-polaron interaction, and device degradation.^{31,68–71} Measuring aggregation in OLED active layers is a natural problem for APT, which can easily discriminate and locate each molecule with high precision. To study aggregation, we deposited a blended film of 6% (vol. %) Ir(ppy)₃ in CBP—a typical blend ratio for this system.⁷¹

To characterize clustering of Ir(ppy)₃ in the sample,

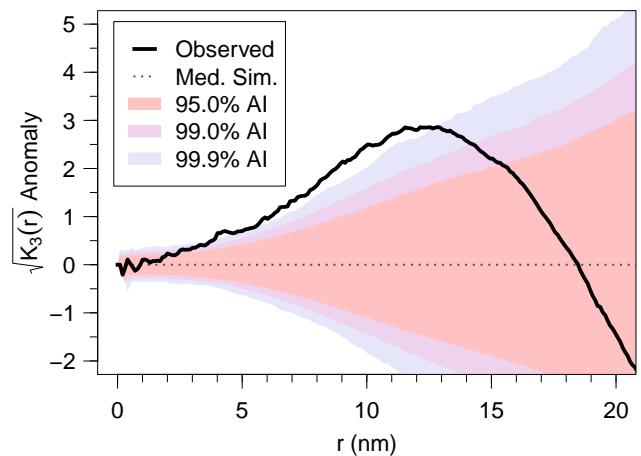


Figure 6. K-function anomaly for Ir(ppy)₃ in CBP along with simulation envelopes. The excursion of the observed K-function above the envelopes indicates significant (deviation outside a 99.9% acceptance interval) clustering of the Ir(ppy)₃ in the range of about 5 nm to 12 nm.

we used the three-dimensional K-function (K_3); this function measures the number of additional Ir(ppy)₃ molecules contained within a sphere of radius r centered about each Ir(ppy)₃ molecule, normalized by the bulk concentration of Ir(ppy)₃.⁷² Acceptance interval envelopes were generated for the measured K-function by randomly relabeling the molecular identities of the measured CBP:Ir(ppy)₃ data 50,000 times and calculating $K_3(r)$ of the relabeled Ir(ppy)₃ patterns. Deviations above this envelope indicate significant non-random clustering of the observed Ir(ppy)₃ at those distances.

We use the square root of the K-function to stabilize the variance of the envelopes; this transformation does not change any of the underlying conclusions drawn about the observed data, and is commonly used in the analysis of point patterns.^{72,73} To make interpretation of the data easier, we also subtract the median value of the envelope, centering the plot about zero. From the transformed K-function and envelopes shown in Figure 6, we observe significant (deviation outside a 99.9% acceptance interval) clustering of the Ir(ppy)₃ in the range of about 5 nm to 12 nm. This corroborates earlier work using HAADF-STEM,³¹ but adds quantitative length scales in three dimensions that allow for better models of mixing and charge transport. Furthermore, the method can be extended to other small-molecule organic systems, as it does not require a high z-contrast atom such as the Ir core in Ir(ppy)₃. The effect of the observed clustering on device properties will be explored in future publications.

III. FUTURE DIRECTIONS

While APT has already provided insights into the structure-property relations of small-molecule organic devices, there are plenty of avenues for improvement. Some

work has been done to use a focused ion beam (FIB) to lift out a section of organic material from a film.^{30,74} Over the last decade or so, this has become the standard method of sample preparation for APT,³⁸ and while this makes sample preparation more challenging, it is similar in complexity to the preparation of organic samples for TEM imaging.²³ If radiation damage can be mitigated, this method should allow for better spatial resolution because it removes the limitation on the radius of curvature to be locally flat, permitting smaller tip radii to enhance spatial resolution (see discussion in Methods section). It also opens up many more avenues for experimentation. In particular, it allows devices to be analyzed after operation, which permits observations of the morphological differences between devices before and after. This would permit experimental testing of models, such as the current filamentation expected during OLED operation.⁷⁵ Similarly, it allows for study of how operation and processing affect morphology, molecular migration, or new chemical species creation due to material reactions.

The spatial information provided for working devices is particularly valuable for closing the experiment-theory loop. Positions of molecules could be fed into a model of electronic transport to directly compare predicted and measured device properties, which would allow rapid testing of models and point to areas of theory that require refinement. Similarly, understanding how molecular structures determine their mixing distributions would help develop a theory of solid-state solubility, directing materials design to control morphology and hence device performance.

IV. CONCLUSIONS

Morphology is inextricably linked to the behavior of organic devices, and it is crucial to understand—and ultimately control—the structures of these systems. Using APT to study small-molecule organic semiconducting systems can potentially answer long-standing questions of device characteristics, and bolster a broader theory of organic electronic physics. The high chemical discrimination (< 1 Da), spatial resolution (~ 0.3 nm in z and ~ 1 nm in x - y), and analytic sensitivity (~ 50 ppm) we have achieved with APT are unmatched for studying the morphology of small-molecule organic materials; we note that these parameters are not fully optimized and there is still room for improvement. Through this chemically-specific and spatially-resolved information, APT can answer questions about both bulk and interfacial structures. This capability adds another powerful characterization tool for the organic electronics community, enabling new experimental directions. As APT matures, it will become an ever more valuable technique for studying organic molecular materials. By providing high-resolution and chemically-specific information, APT can help move organic semiconductors towards their promise of large-scale, high-versatility, and low-cost electronics.

V. METHODS

A. Sample Preparation

Thin films were prepared by vacuum thermal evaporation; film thickness and doping ratios were controlled by the deposition rate, monitored by a quartz crystal oscillator.

CBP and Ir(ppy)₃ were from Lumtec; CBP was used both as received and purified by vacuum gradient sublimation before use, while Ir(ppy)₃ was used as received. Sublimed grade C₆₀ from MER Corp. was purified again with a vacuum gradient sublimation before use. Tetracene was sublimed grade from Sigma Aldrich, used as received.

Because of the sensitivity of organic films to electron radiation, we deposit films directly on a curved Si or W tip rather than using the standard practice of cutting them out from a flat film using a focused ion beam.³⁸ Because of the low evaporation field of molecular organic materials, we can use a tip with a large radius of curvature ($R = 250$ nm to 500 nm) which approximates a flat surface locally. An SEM image of a Si tip is provided in the Supporting Information (Figure S5).

B. Data Acquisition and Analysis

APT data were taken using a CAMECA LEAP 4000X Si operated in laser pulse mode; the multiple hit values are typically below 15%. The reconstructions were performed using CAMECA IVAS software (3.6.14).

Run parameters were optimized to minimize multiple hit events; the parameters presented below are typical for our specimens. The crystalline C₆₀ sample (Figure 4) used a temperature set-point of 30 K, a laser pulse energy of 12 pJ, an evaporation rate target of 1 ion per 100 pulses, a laser pulse frequency of 250 kHz, and a detector distance of 90 mm. It was reconstructed using voltage evolution with an image compression factor (ICF) of 1.60, a detector efficiency of 0.55, and a tip radius of 315 nm. The SDM was generated using 0.05 nm z cuts to give the best peak quality.

The blended CBP:Ir(ppy)₃ sample (Figures 3 & 6) used a temperature set-point of 25 K, a laser pulse energy of 5 pJ, an evaporation rate target of 3 ions per 100 pulses, a laser pulse frequency of 125 kHz, and a detector distance of 160 mm. It was reconstructed using voltage evolution with an ICF of 2.00, a detector efficiency of 0.55, and a tip radius of 350 nm.

A representative voltage curve and detector hit map are provided in the Supporting Information (Figures S6 & S7).

Mass spectra analysis was performed using the MALDIquant package in R, using the Statistics-sensitive Non-linear Iterative Peak-clipping (SNIP) algorithm for background subtraction.⁷⁶ Spatial statistical analysis was

performed using the spatstat package in R, or extensions available at <https://github.com/aproudian2/rapt>.

VI. ACKNOWLEDGMENTS

Work by APP, MBJ, and JDZ was supported by the U.S. Department of Energy (DOE), Office of Science, Basic Energy Sciences (BES) under Award DE-SC0018021. The LEAP was supported by a National Science Foundation Major Research Instrumentation grant DMR-1040456. Renewable Energy Materials Research Science and Engineering Center facilities use was provided by NSF grant DMR-0820518.

VII. SUPPLEMENTAL INFORMATION

The supporting information provides: a multiple hit map (correlation histogram) showing no fragmentation curves for the Ir(ppy)₃:CBP sample, a mass spectrum of as-received CBP and a corresponding correlation histogram similarly showing no fragmentation, a real-space plot of the points used for the SDM with visible lattice planes, an SEM image of a Si sample tip, and a representative detector hit map and voltage curve from APT.

REFERENCES

- ¹D. J. Gaspar, “Materials, Processing, and Applications,” in *OLED Fundamentals: Materials, Devices, and Processing of Organic Light-Emitting Diodes*, edited by D. J. Gaspar and E. Polikarpov (CRC Press, 2015) p. 437.
- ²B. Kippelen and J.-L. Brédas, “Organic Photovoltaics,” *Energy & Environmental Science* **2**, 251–261 (2009).
- ³N. C. Giebink, G. P. Wiederrecht, M. R. Wasielewski, and S. R. Forrest, “Ideal Diode Equation for Organic Heterojunctions. I. Derivation and Application,” *Physical Review B* **82**, 155305 (2010).
- ⁴Y. L. Lin, M. A. Fusella, and B. P. Rand, “The Impact of Local Morphology on Organic Donor/Acceptor Charge Transfer States,” *Advanced Energy Materials* **1702816**, 1702816 (2018).
- ⁵K. Maturová, S. S. Van Bavel, M. M. Wienk, R. A. J. Janssen, and M. Kemerink, “Morphological device model for organic bulk heterojunction solar cells,” *Nano Letters* **9**, 3032–3037 (2009).
- ⁶M. A. Brady, G. M. Su, and M. L. Chabinyc, “Recent progress in the morphology of bulk heterojunction photovoltaics,” *Soft Matter* **7**, 11065 (2011).
- ⁷M. Jørgensen, K. Norrman, and F. C. Krebs, “Stability/degradation of polymer solar cells,” *Solar Energy Materials and Solar Cells* **92**, 686–714 (2008).
- ⁸C. Groves, O. G. Reid, and D. S. Ginger, “Heterogeneity in Polymer Solar Cells: Local Morphology and Performance in Organic Photovoltaics Studied with Scanning Probe Microscopy,” *Accounts of Chemical Research* **43**, 612–620 (2010).
- ⁹A. R. G. Smith, J. L. Ruggles, H. Cavaye, P. E. Shaw, T. a. Darwish, M. James, I. R. Gentle, and P. L. Burn, “Investigating morphology and stability of fac-tris (2-phenylpyridyl) iridium(III) films for OLEDs,” *Advanced Functional Materials* **21**, 2225–2231 (2011).
- ¹⁰W. L. Leong, G. C. Welch, J. Seifert, J. H. Seo, G. C. Bazan, and A. J. Heeger, “Understanding the role of thermal processing in high performance solution processed small molecule bulk heterojunction solar cells,” *Advanced Energy Materials* **3**, 356–363 (2013).
- ¹¹A. Neuhold, H. Brandner, S. J. Ausserlechner, S. Lorbeck, M. Neuschitzer, E. Zojer, C. Teichert, and R. Resel, “X-ray based tools for the investigation of buried interfaces in organic electronic devices,” *Organic Electronics* **14**, 479–487 (2013).
- ¹²K. Vandewal, S. Himmelberger, and A. Salleo, “Structural Factors That Affect the Performance of Organic Bulk Heterojunction Solar Cells,” *Macromolecules* **46**, 6379–6387 (2013).
- ¹³Y.-T. Fu, D. A. da Silva Filho, G. Sini, A. M. Asiri, S. G. Aziz, C. Risko, and J.-L. Brédas, “Structure and Disorder in Squaraine-C60 Organic Solar Cells: A Theoretical Description of Molecular Packing and Electronic Coupling at the Donor-Acceptor Interface,” *Advanced Functional Materials* **24**, 3790–3798 (2014).
- ¹⁴S. Lan, H. Yang, G. Zhang, X. Wu, W. Ning, S. Wang, H. Chen, and T. Guo, “Impact of Fullerene Structure on Nanoscale Morphology and Miscibility and Correlation of Performance on Small Molecules: Fullerene Solar Cell,” *The Journal of Physical Chemistry C*, acs.jpcc.6b08025 (2016).
- ¹⁵J. Vinokur, S. Obuchovsky, I. Deckman, L. Shoham, T. Mates, M. L. Chabinyc, and G. L. Frey, “Dynamics of Additive Migration to Form Cathodic Interlayers in Organic Solar Cells,” *ACS Applied Materials & Interfaces* **9**, 29889–29900 (2017).
- ¹⁶B. W. D’Andrade, S. R. Forrest, and A. B. Chwang, “Operational stability of electrophosphorescent devices containing p and n doped transport layers,” *Applied Physics Letters* **83**, 3858–3860 (2003).
- ¹⁷I. R. De Moraes, S. Scholz, B. Lüssem, and K. Leo, “Chemical degradation processes of highly stable red phosphorescent organic light emitting diodes,” *Organic Electronics* **13**, 1900–1907 (2012).
- ¹⁸Y. J. Cho, Y. Zhang, H. Yu, and H. Aziz, “The Root Causes of the Limited Stability of Solution-Coated Small-Molecule Organic Light-Emitting Devices: Faster Host Aggregation by Exciton-Polaron Interactions,” *Advanced Functional Materials* (2016).
- ¹⁹I. Fraga Domínguez, A. Distler, and L. Lüer, “Stability of Organic Solar Cells: The Influence of Nanostructured Carbon Materials,” *Advanced Energy Materials* **7** (2017).
- ²⁰W. R. Mateker and M. D. McGehee, “Progress in Understanding Degradation Mechanisms and Improving Stability in Organic Photovoltaics,” *Advanced Materials* **29**, 1603940 (2017).
- ²¹S. C. Dong, L. Xu, and C. W. Tang, “Chemical degradation mechanism of TAPC as hole transport layer in blue phosphorescent OLED,” *Organic Electronics* **42**, 379–386 (2017).
- ²²J. S. Bangsund, K. W. Hershey, and R. J. Holmes, “Isolating Degradation Mechanisms in Mixed Emissive Layer Organic Light-Emitting Devices,” *ACS Applied Materials & Interfaces* **10**, 5693–5699 (2018).
- ²³W. Chen, M. P. Nikiforov, and S. B. Darling, “Morphology characterization in organic and hybrid solar cells,” *Energy & Environmental Science* **5**, 8045 (2012).
- ²⁴M. Pfannmöller, W. Kowalsky, and R. R. Schröder, “Visualizing physical, electronic, and optical properties of organic photovoltaic cells,” *Energy & Environmental Science* **6**, 2871 (2013).
- ²⁵J. D. Roehling, K. J. Batenburg, F. B. Swain, A. J. Moulé, and I. Arslan, “Three-Dimensional Concentration Mapping of Organic Blends,” *Advanced Functional Materials* **23**, 2115–2122 (2013).
- ²⁶E. M. Tennyson, J. M. Howard, and M. S. Leite, “Mesoscale Functional Imaging of Materials for Photovoltaics,” *ACS Energy Letters* **2**, 1825–1834 (2017).
- ²⁷A. Neuhold, J. Novák, H. G. Flesch, A. Moser, T. Djuric, L. Grodd, S. Grigorian, U. Pietsch, and R. Resel, “X-ray radiation damage of organic semiconductor thin films during grazing incidence diffraction experiments,” *Nuclear Instruments and Methods in Physics Research, Section B: Beam Interactions with Materials and Atoms* **284**, 64–68 (2012).
- ²⁸W. Schindler, M. Wollgarten, and K. Fostiropoulos, “Revealing nanoscale phase separation in small-molecule photovoltaic

- blends by plasmonic contrast in the TEM,” *Organic Electronics* **13**, 1100–1104 (2012).
- ²⁹J. A. Love, C. M. Proctor, J. Liu, C. J. Takacs, A. Sharengo, T. S. Van Der Poll, A. J. Heeger, G. C. Bazan, and T. Q. Nguyen, “Film morphology of high efficiency solution-processed small-molecule solar cells,” *Advanced Functional Materials* **23**, 5019–5026 (2013).
- ³⁰A. Orthacker, R. Schmied, B. Chernev, J. E. Fröch, R. Winkler, J. Hobisch, G. Trimmel, and H. Plank, “Chemical degradation and morphological instabilities during focused ion beam prototyping of polymers,” *Phys. Chem. Chem. Phys.* **16**, 1658–1666 (2014).
- ³¹S. Reineke, G. Schwartz, K. Walzer, M. Falke, and K. Leo, “Highly phosphorescent organic mixed films: The effect of aggregation on triplet-triplet annihilation,” *Applied Physics Letters* **94**, 2007–2010 (2009).
- ³²D. Deng, Y. Zhang, J. Zhang, Z. Z. Wang, L. Zhu, J. Fang, B. Xia, Z. Z. Wang, K. Lu, W. Ma, and Z. Wei, “Fluorination-enabled optimal morphology leads to over 11% efficiency for inverted small-molecule organic solar cells,” *Nature Communications* **7**, 1–9 (2016).
- ³³S. V. Vickers, H. Barcena, K. A. Knights, R. K. Thomas, J. C. Ribierre, S. Gambino, I. D. W. Samuel, P. L. Burn, and G. Fragneto, “Light-emitting dendrimer film morphology: A neutron reflectivity study,” *Applied Physics Letters* **96**, 4–7 (2010).
- ³⁴S. E. Shaheen, C. J. Brabec, N. S. Sariciftci, F. Padinger, T. Fromherz, and J. C. Hummelen, “2.5% Efficient Organic Plastic Solar Cells,” *Applied Physics Letters* **78**, 841 (2001).
- ³⁵J. K. van Duren, X. Yang, J. Loos, C. W. T. Bulle-Lieuwma, A. B. Sieval, J. C. Hummelen, and R. A. Janssen, “Relating The Morphology Of Poly(P-Phenylene Vinylene)/Methanofullerene Blends To Solar-Cell Performance,” *Advanced Functional Materials* **14**, 425–434 (2004).
- ³⁶C. R. McNeill, C. J. Fell, J. L. Holdsworth, and P. C. Dastoor, “Screening for artifacts in near-field scanning photocurrent microscopy images of polymer solar cells,” *Synthetic Metals* **153**, 85–88 (2005).
- ³⁷N. J. Popczun, L. Breuer, A. Wucher, and N. Winograd, “On the SIMS Ionization Probability of Organic Molecules,” *Journal of The American Society for Mass Spectrometry* **28**, 1182–1191 (2017).
- ³⁸T. F. Kelly and M. K. Miller, “Invited Review Article: Atom Probe Tomography,” *Review of Scientific Instruments* **78**, 031101 (2007).
- ³⁹T. F. Kelly and D. J. Larson, “Atom Probe Tomography 2012,” *Annual Review of Materials Research* **42**, 1–31 (2012).
- ⁴⁰R. M. Ulfing, T. J. Prosa, Y. Chen, K. P. Rice, I. Martin, D. A. Reinhard, B. P. Gieser, E. Oltman, D. R. Lenz, J. Bunton, M. Van Dyke, T. F. Kelly, and D. J. Larson, “Hardware and Software Advances in Commercially Available Atom Probe Tomography Systems,” *Microscopy and Microanalysis* **23**, 40–41 (2017).
- ⁴¹B. P. Geiser, T. F. Kelly, D. J. Larson, J. Schneir, and J. P. Roberts, “Spatial Distribution Maps for Atom Probe Tomography,” *Microscopy and Microanalysis* **13**, 437–447 (2007).
- ⁴²P. Bas, A. Bostel, B. Deconihout, and D. Blavette, “A general protocol for the reconstruction of 3D atom probe data,” *Applied Surface Science* **87–88**, 298–304 (1995).
- ⁴³E. Machlin, A. Freilich, D. Agrawal, J. Burton, and C. Briant, “Field ion microscopy of biomolecules,” *Journal of Microscopy* **104**, 127–168 (1975).
- ⁴⁴J. A. Panitz, “Point-Projection Imaging of Unstained Ferritin Clusters,” *Ultramicroscopy* **7**, 241–248 (1982).
- ⁴⁵J. A. Panitz, “Direct Visualization of Unstained Nucleic Acids on a Metal Substrate,” *Ultramicroscopy* **11**, 161–166 (1983).
- ⁴⁶O. Nishikawa, T. Sekine, Y. Ohtani, K. Maeda, Y. Numada, and M. Watanabe, “Atomic Investigation of Individual Apexes of Diamond Emitters by a Scanning Atom Probe,” *Journal of Vacuum Science & Technology B* **16**, 836–840 (1998).
- ⁴⁷O. Nishikawa and H. Kato, “Atom-probe study of a conducting polymer: The oxidation of polypyrrole,” *The Journal of Chemical Physics* **85**, 6758–6764 (1986).
- ⁴⁸T. Maruyama, Y. Hasegawa, T. Nishi, and T. Sakurai, “FIM AND ATOM-PROBE STUDY OF POLYMERS,” *Le Journal de Physique Colloques* **48**, C6–269–C6–274 (1987).
- ⁴⁹Y. Zhang, *Three Dimensional Atom Probe Tomography of Nanoscale Thin Films, Interfaces and Particles*, Ph.D. thesis, Iowa State University (2009).
- ⁵⁰T. J. Prosa, S. K. Keeney, and T. F. Kelly, “Atom Probe Tomography Analysis of poly(3-alkylthiophene)s,” *Journal of Microscopy* **237**, 155–67 (2010).
- ⁵¹D. Joester, A. Hillier, Y. Zhang, and T. J. Prosa, “Organic Materials and Organic/Inorganic Heterostructures in Atom Probe Tomography,” *Microscopy Today* **20**, 26–31 (2012).
- ⁵²B. Gault, M. P. Moody, J. M. Cairney, and S. P. Ringer, *Atom Probe Microscopy* (Springer, 2012).
- ⁵³F. De Geuser, B. Gault, A. Bostel, and F. Vurpillot, “Correlated field evaporation as seen by atom probe tomography,” *Surface Science* **601**, 536–543 (2007).
- ⁵⁴D. W. Saxey, “Correlated ion analysis and the interpretation of atom probe mass spectra,” *Ultramicroscopy* **111**, 473–479 (2011).
- ⁵⁵A. Hinderhofer, A. Gerlach, K. Broch, T. Hosokai, K. Yonezawa, K. Kato, S. Kera, N. Ueno, and F. Schreiber, “Geometric and Electronic Structure of Templated C60 on Diindenopyrene Thin Films,” *The Journal of Physical Chemistry C* **117**, 1053–1058 (2013).
- ⁵⁶B. Gault, M. P. Moody, F. de Geuser, D. Haley, L. T. Stephenson, and S. P. Ringer, “Origin of the Spatial Resolution in Atom Probe Microscopy,” *Applied Physics Letters* **95**, 034103 (2009).
- ⁵⁷D. J. Larson, T. J. Prosa, R. M. Ulfing, B. P. Geiser, and T. F. Kelly, *Local Electrode Atom Probe Tomography* (Springer, New York, 2013).
- ⁵⁸A. P. Proudian, M. B. Jaskot, C. Lyiza, D. R. Diercks, B. P. Gorman, and J. D. Zimmerman, “Effect of Diels–Alder Reaction in C 60 -Tetracene Photovoltaic Devices,” *Nano Letters* **16**, 6086–6091 (2016).
- ⁵⁹F. Cataldo, D. A. García-hernández, and A. Manchado, “A Study on the Synthesis and Stability of the C60 Fullerene/Tetracene Adduct,” *European Chemical Bulletin* **3**, 740–744 (2014).
- ⁶⁰T. Breuer, A. Karthäuser, and G. Witte, “Effects of Molecular Orientation in Acceptor-Donor Interfaces between Pentacene and C 60 and Diels-Alder Adduct Formation at the Molecular Interface,” *Advanced Materials Interfaces* **3** (2016).
- ⁶¹Y. Murata, N. Karo, K. Fujiwara, and K. Komatsu, “Solid-state [4 + 2] cycloaddition of fullerene C60 with condensed aromatics using a high-speed vibration milling technique,” *Journal of Organic Chemistry* **64**, 3483–3488 (1999).
- ⁶²F. L. Liu, P. P. Ruden, I. H. Campbell, D. L. Smith, P. Paul Ruden, I. H. Campbell, and D. L. Smith, “Device model for electronic processes at organic/organic interfaces,” *Journal of Applied Physics* **111**, 94507 (2012).
- ⁶³W. C. Herndon and L. H. Hall, “Endo and Exo Transition States in the Diels-Alder Reaction,” *Tetrahedron Letters* , 3095–3100 (1967).
- ⁶⁴K. Drexage and F. Schafer, “Dye Laser,” in *Topics in Applied Physics* (Springer-Verlag, 1977) 1st ed.
- ⁶⁵D. Lutz, K. A. Nelson, C. Gochanour, and M. Fayer, “Electronic excited state energy transfer, trapping by dimers and fluorescence quenching in concentrated dye solutions: Picosecond transient grating exp,” *Chemical Physics* **58**, 325–334 (1981).
- ⁶⁶C. W. Tang, S. A. Vanslyke, and C. H. Chen, “Electroluminescence of doped organic thin films,” *Journal of Applied Physics* **65**, 3610–3616 (1989).
- ⁶⁷C. W. Tang and S. A. Vanslyke, “Organic electroluminescent diodes,” *Applied Physics Letters* **51**, 913–915 (1987).
- ⁶⁸M. A. Baldo, D. F. O’Brien, and S. R. Forrest, “Excitonic singlet-triplet ratio in a semiconducting organic thin film,” *Physical Review B* **60**, 14422–14428 (1999).

- ⁶⁹S. Lamansky, P. I. Djurovich, D. Murphy, F. Abdel-Razzaq, H. E. Lee, C. Adachi, P. E. Burrows, S. R. Forrest, and M. E. Thompson, "Highly phosphorescent bis-cyclometalated iridium complexes: Synthesis, photophysical characterization, and use in organic light emitting diodes," *Journal of the American Chemical Society* **123**, 4304–4312 (2001).
- ⁷⁰Y. Kawamura, J. Brooks, J. J. Brown, H. Sasabe, and C. Adachi, "Intermolecular interaction and a concentration-Quenching mechanism of phosphorescent Ir(III) complexes in a solid film," *Physical Review Letters* **96**, 11–14 (2006).
- ⁷¹Y. Divayana and X. W. Sun, "Observation of excitonic quenching by long-range dipole-dipole interaction in sequentially doped organic phosphorescent host-guest system," *Physical Review Letters* **99**, 1–4 (2007).
- ⁷²B. D. Ripley, "Modelling Spatial Patterns," *Journal of the Royal Statistical Society* **39**, 172–212 (1977).
- ⁷³A. J. Baddeley, E. Rubak, and R. Turner, *Spatial Point Patterns: Methodology and Applications with R* (CRC Press, Boca Raton, 2016).
- ⁷⁴S. Kim, M. Jeong Park, N. P. Balsara, G. Liu, and A. M. Minor, "Minimization of focused ion beam damage in nanostructured polymer thin films," *Ultramicroscopy* **111**, 191–199 (2011).
- ⁷⁵Y. Shen and N. C. Giebink, "Monte Carlo Simulations of Nanoscale Electrical Inhomogeneity in Organic Light-Emitting Diodes and Its Impact on Their Efficiency and Lifetime," *Physical Review Applied* **4**, 054017 (2015).
- ⁷⁶M. Morháč, "An Algorithm for Determination of Peak Regions and Baseline Elimination in Spectroscopic Data," *Nuclear Instruments and Methods in Physics Research Section A: Accelerators, Spectrometers, Detectors and Associated Equipment* **600**, 478–487 (2009).

**Atom Probe Tomography of Organic Molecular Materials: Sub-Dalton
Nanometer-Scale Quantification –
Supplemental Information**

Andrew P. Proudian,¹ Matthew B. Jaskot,² David R. Diercks,^{2,3} Brian P. Gorman,^{2,3}
and Jeramy D. Zimmerman^{1,2}

¹*Department of Physics, Colorado School of Mines*

²*Materials Science Program, Colorado School of Mines*

³*Department of Metallurgical and Materials Engineering,
Colorado School of Mines*

(Dated: December 14, 2024)

I. CORRELATION HISTOGRAMS

Correlation histograms of events when two ions are detected for a single laser pulse were proposed by Saxey to aid in mass spectrum analysis for atom probe tomography (APT).¹ It plots the masses (i & j) of each detection event against each other and then bins this data to examine occurrence frequencies; as a result, it is symmetric about $i = j$.

There are four key features that are visible in correlation histograms. First are the expected bright spots at coincidences between major peaks i and j representing the field evaporation of two ions. More interesting are the three types of lines that emanate from these points. Horizontal and vertical lines are due to the delayed evaporation of one ion of the pair. Curved tracks that go from low i and j (lower left) to high i and j (upper right) are the result of delayed evaporation for both ions. Finally, tracks that go from upper left to lower right are due to mid-flight dissociation of the parent ion, which are of interest when investigating possible molecular fragmentation.

II. IMPURITY

For the blended film of 6 vol % tris[2-phenylpyridinato-C2,N]iridium(III) ($\text{Ir}(\text{ppy})_3$) in 4,4'-bis(N-carbazolyl)-1,1'-biphenyl (CBP, purified by thermal gradient sublimation), there are three pieces of evidence that support assignment of the peak at 169 Da as an impurity over a fragment. First is the mass detected in the inset of Figure 3 indicating the presence of H at the possible fragmentation location. Second is a correlation histogram of the data showing no evidence of fragmentation of the doubly ionized CBP into that peak (Figure S1). Third is the relative component of the peak is an order of magnitude higher in the as-received material (5 %) (Figure S2) as compared to the purified (0.5 %) (Figure 3). In this film, with much a higher signal from this impurity peak, there is still no evidence of fragmentation in a correlation histogram (Figure S3).

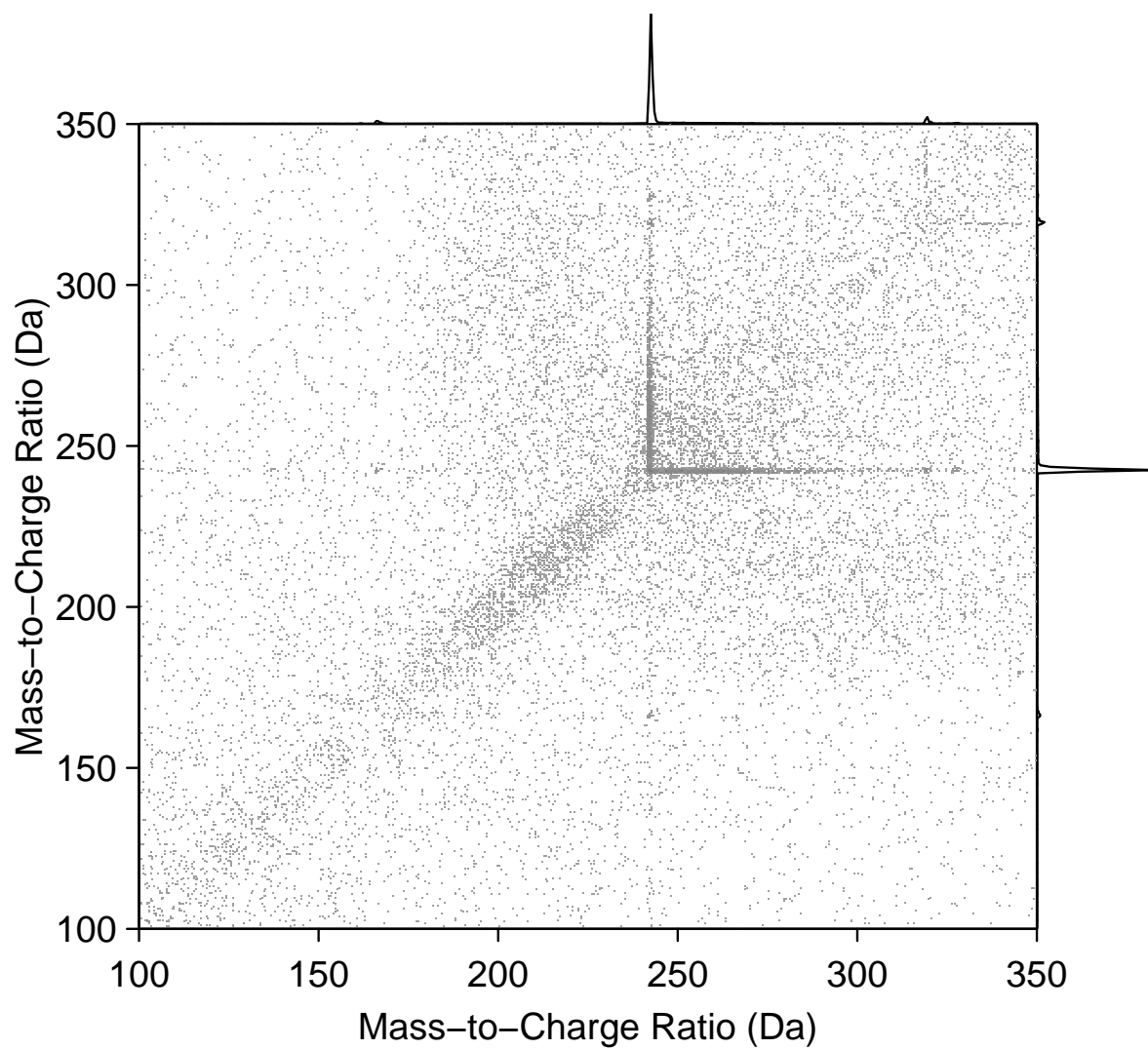


Figure S1. A correlation histogram of a blended film of 6 vol% tris[2-phenylpyridinato-C2,N]iridium(III) ($\text{Ir}(\text{ppy})_3$) in 4,4'-bis(N-carbazolyl)-1,1'-biphenyl (CBP, purified by thermal gradient sublimation) focused on the CBP^{++} peak, which shows no evidence of fragmentation of the CBP into the unexpected peaks.

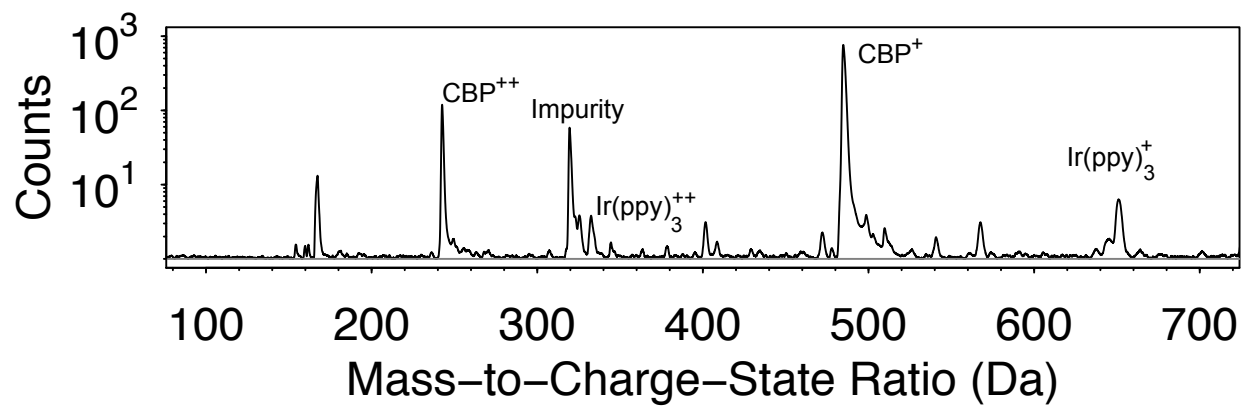


Figure S2. Mass spectrum of as-received CBP; the impurity at 319 Da is 5% as compared to 0.5% in the CBP purified by thermal gradient sublimation used in the 6 vol% Ir(ppy)₃:CBP blend.

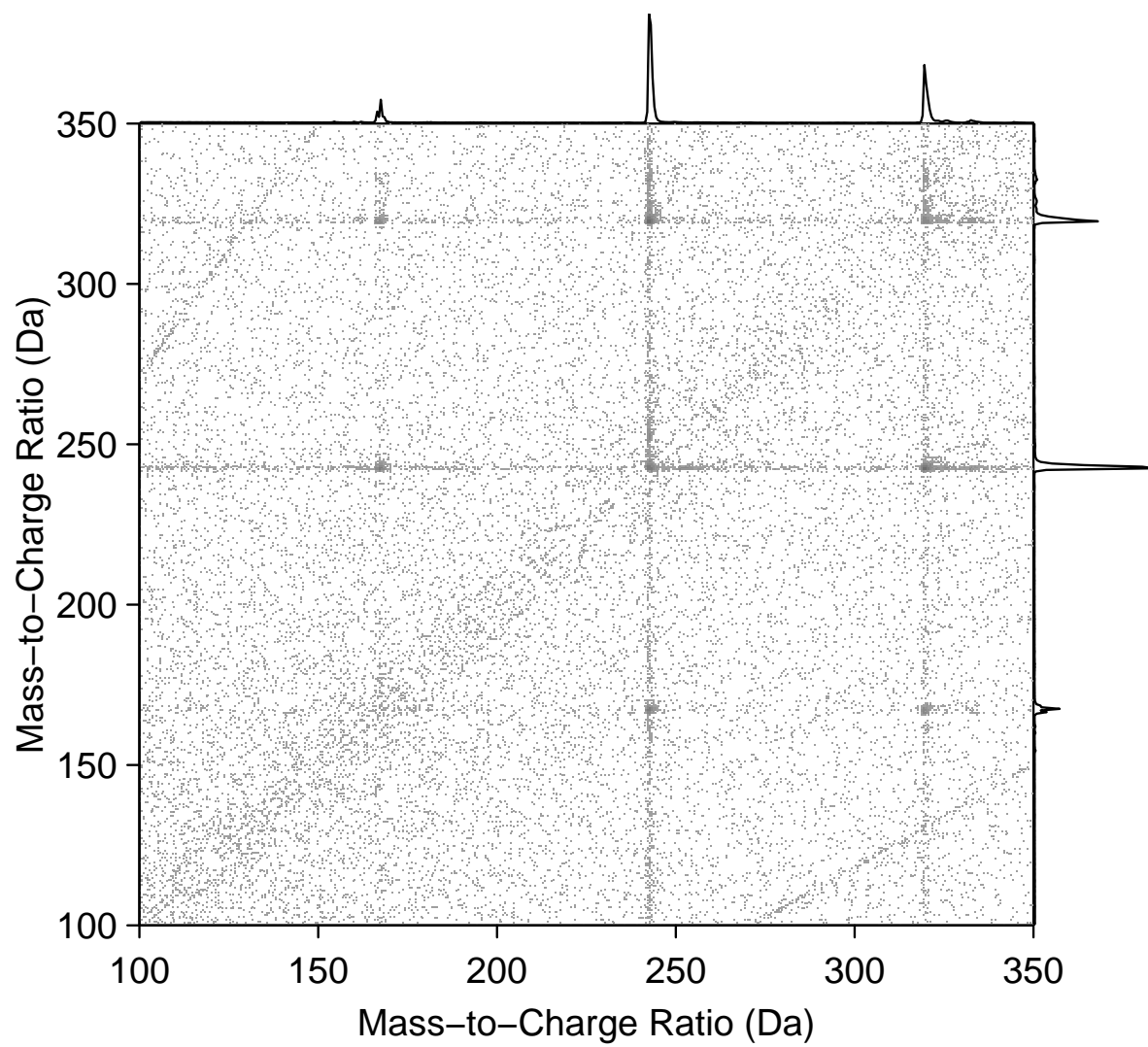


Figure S3. A correlation histogram of the as-received CBP focused on the CBP^{++} peak at 242 Da, which shows no evidence of fragmentation of the CBP into the unexpected peaks.

III. ATOM PROBE

We use a smooth Si tip as the substrate for our APT sample films (Figure S5). These tips, though very large compared to a typical APT sample radius of curvature,² still yield smooth evaporation both spatially and temporally. Figure S6 shows the smooth variation of hits across the detector, and Figure S7 shows the narrow window of voltage used during APT. We note that the fluctuations in voltage during the run are due to laser drift compensation algorithm errors, requiring manual laser adjustments to keep the sample properly running; this leads to more abrupt changes in evaporation rate and hence voltage than in typical APT runs.

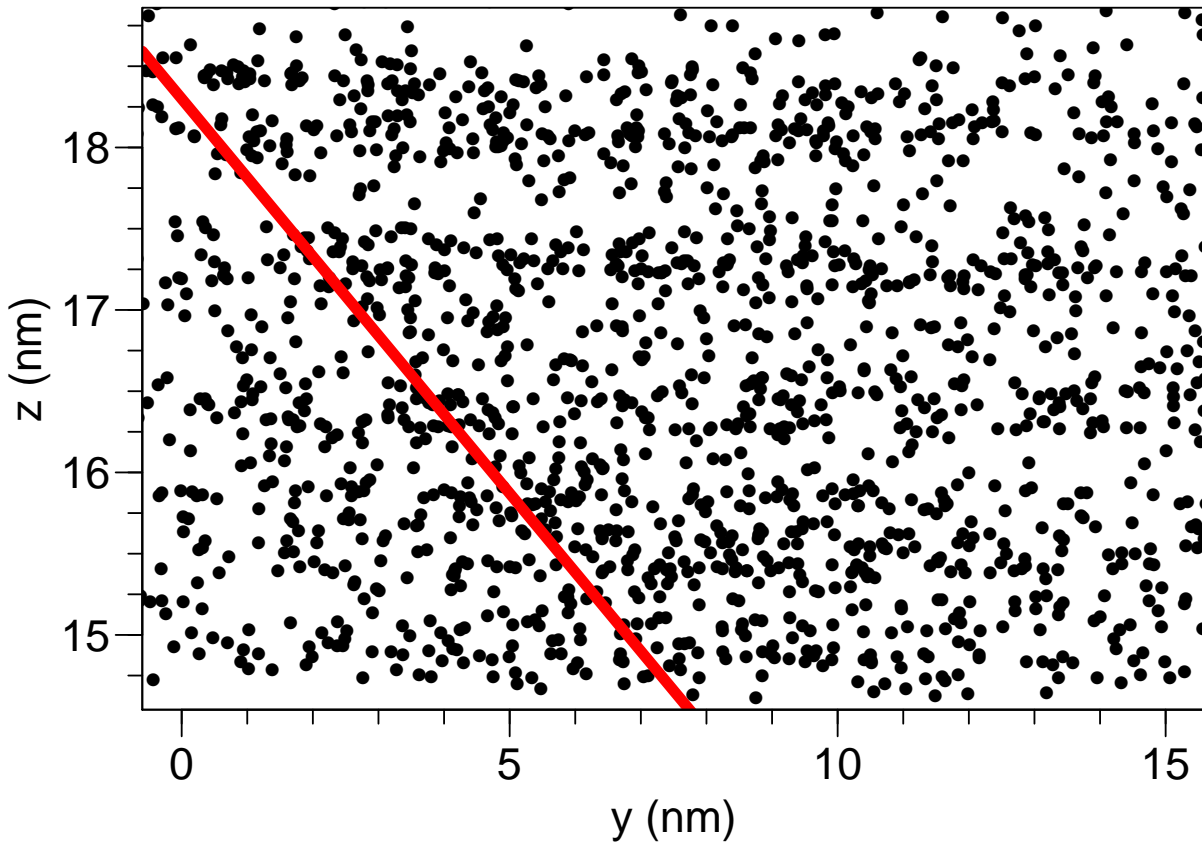


Figure S4. A real space plot of the points used to generate the spatial distribution map (SDM) in Figure 4. The red line marks the location of a potential grain boundary.

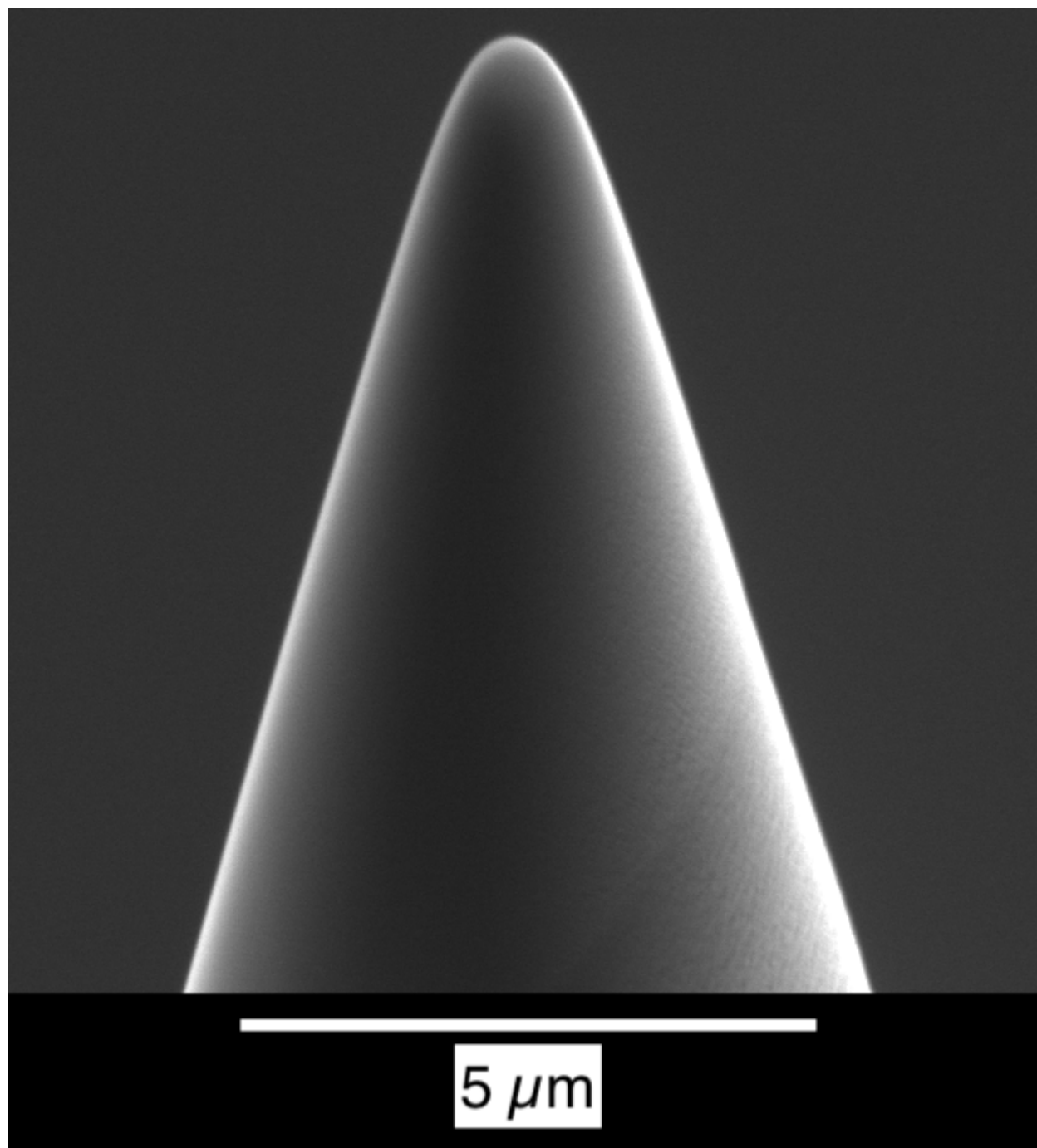


Figure S5. A representative Si tip used for film deposition and subsequent atom probe tomography (APT) analysis.

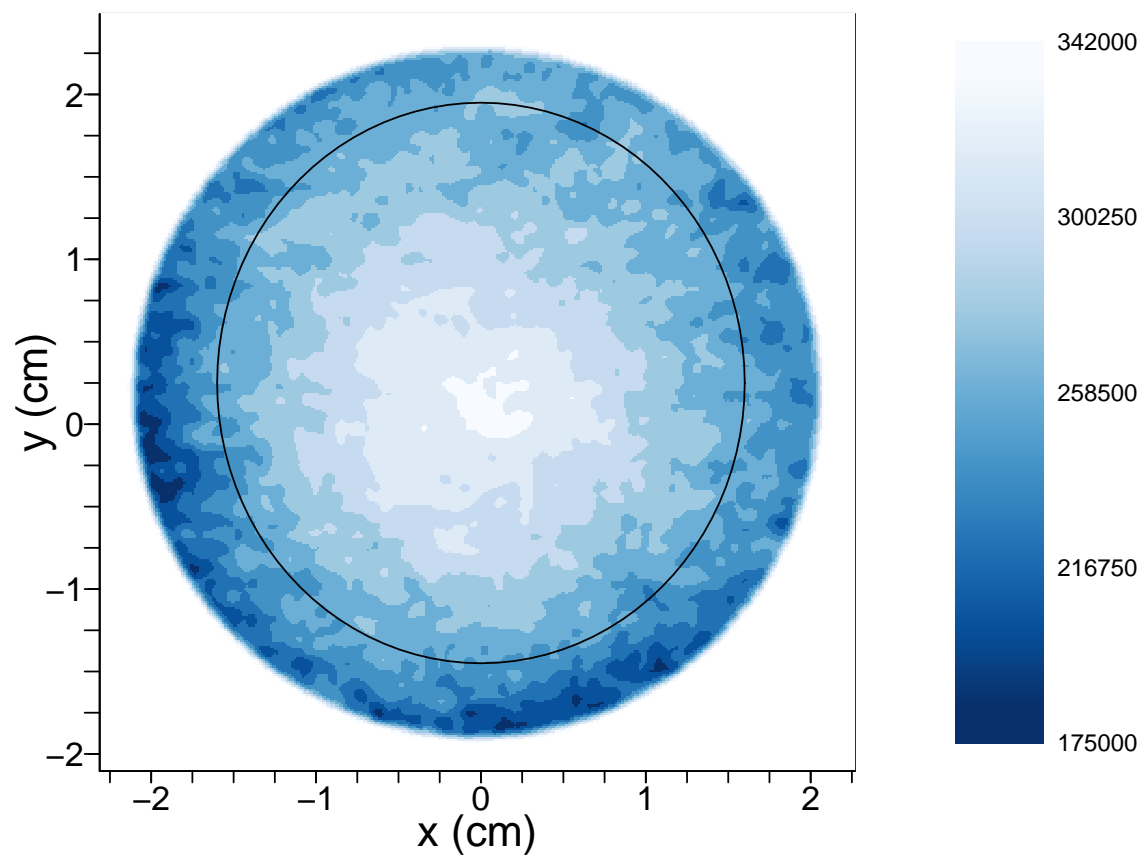


Figure S6. A representative detector hit map for small-molecule organic semiconductor samples.

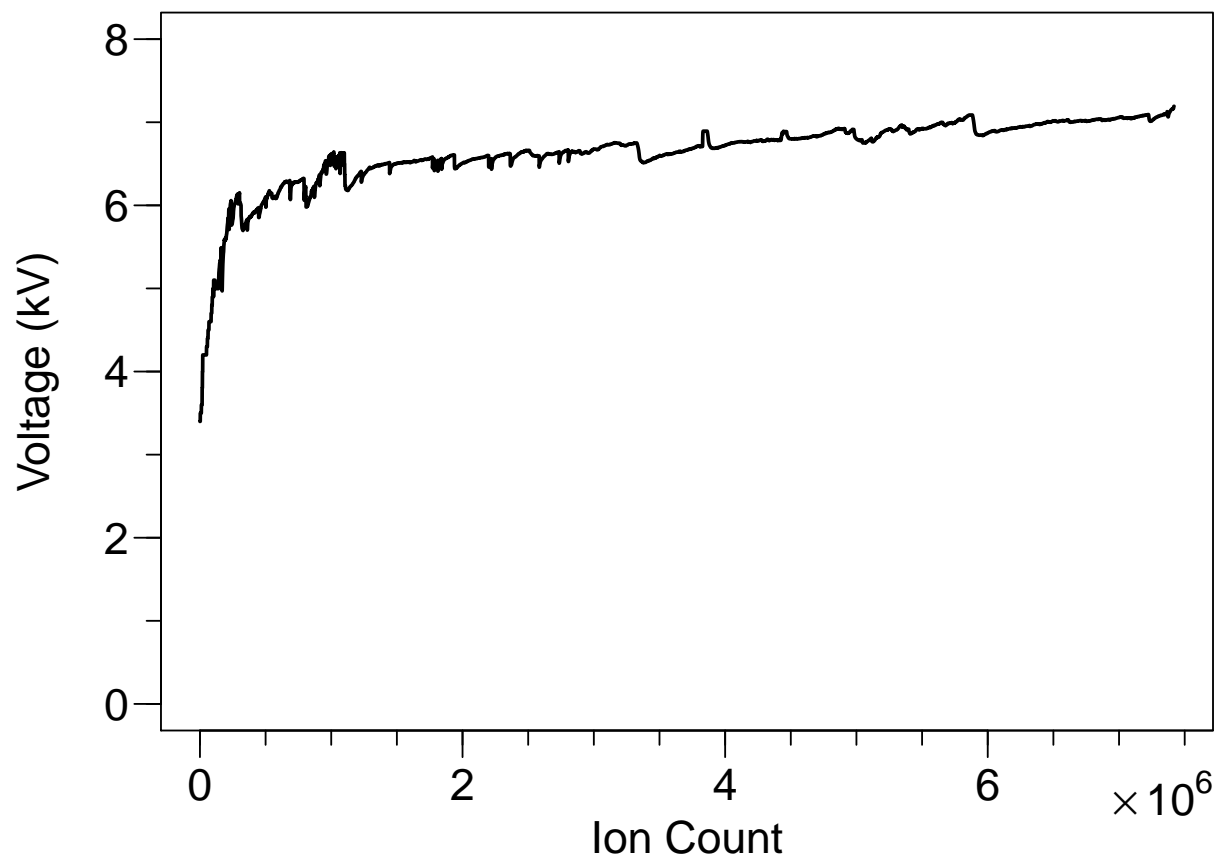


Figure S7. A representative voltage curve for small-molecule organic semiconductor samples. The fluctuations in the curve are due to the laser drift compensation algorithm not working effectively for our sample geometry, requiring manual laser adjustments to keep the sample properly running.

REFERENCES

- ¹D. W. Saxey, “Correlated ion analysis and the interpretation of atom probe mass spectra,” *Ultramicroscopy* **111**, 473–479 (2011).
- ²T. F. Kelly and D. J. Larson, “Atom Probe Tomography 2012,” *Annual Review of Materials Research* **42**, 1–31 (2012).